

Multiplexing technology based on SQUID for readout of superconducting transition-edge sensor arrays

Xinyu Wu(吴歆宇), Qing Yu(余晴), Yongcheng He(何永成), Jianshe Liu(刘建设), and Wei Chen(陈炜)
Citation: Chin. Phys. B, 2022, 31 (**10**): 108501. DOI: 10.1088/1674-1056/ac693c
Journal homepage: http://cpb.iphy.ac.cn; http://iopscience.iop.org/cpb

What follows is a list of articles you may be interested in

Development of series SQUID array with on-chip filter for TES detector

Wentao Wu(伍文涛), Zhirong Lin(林志荣), Zhi Ni(倪志), Peizhan Li(李佩展), Tiantian Liang(梁恬恬), Guofeng Zhang(张国峰), Yongliang Wang(王永良), Liliang Ying(应利良), Wei Peng(彭炜), Wen Zhang(张文), Shengcai Shi(史生才), Lixing You(尤立星), and Zhen Wang(王镇)
Chin. Phys. B, 2022, 31 (**2**): 028504. DOI: 10.1088/1674-1056/ac2b91

Temperature and current sensitivity extraction of optical superconducting transition-edge sensors based on a two-fluid model

Yue Geng(耿悦), Pei-Zhan Li(李佩展), Jia-Qiang Zhong(钟家强), Wen Zhang(张文), Zheng Wang(王争), Wei Miao(缪巍), Yuan Ren(任远), and Sheng-Cai Shi(史生才)
Chin. Phys. B, 2021, 30 (**9**): 098501. DOI: 10.1088/1674-1056/ac11ce

Low-T_c direct current superconducting quantum interference device magnetometer-based 36-channel magnetocardiography system in a magnetically shielded room

Qiu Yang, Li Hua, Zhang Shu-Lin, Wang Yong-Liang, Kong Xiang-Yan, Zhang Chao-Xiang, Zhang Yong-Sheng, Xu Xiao-Feng, Yang Kang, Xie Xiao-Ming
Chin. Phys. B, 2015, 24 (**7**): 078501. DOI: 10.1088/1674-1056/24/7/078501

Optical response of Al/Ti bilayer transition edge sensors

Zhang Qing-Ya, Wang Tian-Shun, Liu Jian-She, Dong Wen-Hui, He Gen-Fang, Li Tie-Fu, Zhou Xing-Xiang, Chen Wei
Chin. Phys. B, 2014, 23 (**11**): 118502. DOI: 10.1088/1674-1056/23/11/118502

Superconducting quantum interference devices with different damped junctions operated in directly coupled current- and voltage-bias modes

Zeng Jia, Zhang Yi, Qiu Yang, Zhang Guo-Feng, Wang Yong-Liang, Kong Xiang-Yan, Xie Xiao-Ming
Chin. Phys. B, 2014, 23 (**11**): 118501. DOI: 10.1088/1674-1056/23/11/118501

REVIEW

Multiplexing technology based on SQUID for readout of superconducting transition-edge sensor arrays

Xinyu Wu(吴歆宇), Qing Yu(余晴), Yongcheng He(何永成), Jianshe Liu(刘建设), and Wei Chen(陈炜)†

School of Integrated Circuits, Tsinghua University, Beijing 100084, *China*

(Received 29 March 2022; revised manuscript received 20 April 2022; accepted manuscript online 22 April 2022)

Multiplexing technologies based on superconducting quantum interference devices (SQUIDs) are crucial to cryogenic readout of superconducting transition-edge sensor (TES) arrays. Demands for large-scale TES arrays promote the development of multiplexing technologies towards large multiplexing factors and low readout noise. The development of multiplexing technologies also facilitates new applications of TES arrays in a wide range of frequencies. Here we summarize different types of SQUID-based multiplexing technologies including time-division multiplexing, code-division multiplexing, frequency-division multiplexing and microwave SQUID multiplexing. The advances and parameter constraints of each multiplexing technology are also discussed.

Keywords: superconducting transition-edge sensor arrays, superconducting quantum interference devices, multiplexing technology, cryogenic readout

PACS: 85.25.Oj, 85.25.Dq, 07.20.Fw, 07.57.Kp **DOI:** 10.1088/1674-1056/ac693c

1. Introduction

Superconducting transition-edge sensors (TESs) are highly sensitive for incident energy or power at cryogenic temperatures. Since TESs are applicable to a broad wavelength range, cryogenic detectors based on TESs have a wide range of applications. TES microcalorimeters can achieve excellent energy resolution when detecting high-energy photons such as x rays and gamma rays.[1–5] TES bolometers are widely used in cosmic microwave background (CMB) experiments due to low noise level and good response linearity.[6–10] TES single photon detectors have high detection efficiency and photon-number-resolving capability, which can meet the measurement requirements in the field of quantum optics.[11–15] These applications drive the development of large-scale TES arrays to further improve collection efficiency, counting rate and sensitivity of TESs. Superconducting quantum interference devices (SQUIDs) are one of the most sensitive sensors of magnetic flux, which are typically used as amplifiers to detect physical quantities that can be converted into magnetic flux.[16] Because the SQUID amplifier has low input impedance, low noise and low power dissipation, it is preferred for the readout of the TES detector.[17,18]

However, as the number of TES detectors in the array increases, the complexity of wiring and the thermal load pose great challenges to the cryogenic readout. Therefore, it is essential to employ SQUID-based multiplexing technologies in which multiple TES detectors share one readout line. The scale of TES arrays largely depends on the number of TES detectors per readout line, which is referred to as the multiplexing factor. To increase the scale of TES arrays and to boost the performance of readout circuits, different multiplexing schemes have been proposed and developed. Currently, these schemes include time-division multiplexing (TDM), code-division multiplexing (CDM), frequency-division multiplexing (FDM) and microwave SQUID multiplexing (MW-Mux). No matter which scheme is employed, the first step is to limit the bandwidth of all TES signals to avoid aliasing of out-of-band noise into the signal bandwidth.[19,20] After bandwidth limitation, TES signals from different channels are combined into a small number of readout lines and transmitted to room-temperature electronics for demodulation and identification. In order to achieve the accurate measurement and the scalable readout of TES signals, these multiplexing schemes focus on improving circuit architectures, electronical components, control algorithms and room temperature hardware. As for applications of various spectrometers and astronomical telescopes, emerging readout systems need to measure thousands of TES detectors while maintaining low readout noise and low crosstalk.

Despite great advances in SQUID-based multiplexing technologies, they still need to be optimized. As the scale of TES arrays continues to extend, the design requirements for multiplexing technologies increase, which mainly focus on the multiplexing factor, readout noise, channel-to-channel crosstalk and operational complexity. Due to parameter constraints in readout circuits, it is difficult for each technology to satisfy the requirements simultaneously. From the perspective

†Corresponding author. E-mail: weichen@tsinghua.edu.cn

© 2022 Chinese Physical Society and IOP Publishing Ltd

of practical applications, the choice of multiplexing technologies is generally a trade-off among these design requirements. In view of this, this paper summarizes the different types of SQUID-based multiplexing technologies and discusses their parameter constraints. The sections are organized as follows: Section 2 briefly introduces the readout circuit of the TES and the orthogonal modulation functions used in different multiplexing technologies. Sections 3–6 describe circuit architectures and parameter constraints of each technology. Section 7 compares characteristics of these multiplexing technologies. Section 8 gives a summary and outlook.

2. Readout circuit of TES

The superconducting transition-edge sensor is essentially a thermistor.[21,22] The measurement of TES signals is of success by measuring the change of TES resistance induced by the energy of incident photons. Figure 1 shows the schematic of the readout circuit of a single TES. In the TES bias circuit, the TES resistance $R_{\rm TES}$ is in parallel with a bias resistor $R_{\rm bias}$ and in series with an input coil $L_{\rm in}$ and a Nyquist coil $L_{\rm Nyq}$. The bias resistor with resistance being much smaller than the TES resistance is used to realize the voltage bias of the TES. The voltage-biased TES operates at the electro-thermal negative feedback (ETF), exhibiting fast response and low noise.[23,24] The Nyquist coil is used to construct an L/R low-pass filter in the TES bias circuit, where the inductance L indicates the total inductance of the input coil and the Nyquist coil, and the resistance R indicates the total resistance of the bias resistor and the TES. This L/R low-pass filter can effectively limit the bandwidth of the TES signal, avoiding the aliasing of high-frequency noise. The current flowing through the TES is inductively coupled to a SQUID (SQ), generating a flux in the SQUID loop. The voltage across the SQUID varies according to the flux-voltage characteristics of the SQUID. Then, the output voltage of the SQUID is transmitted from the cryogenic stage to the room-temperature preamplifier. The role of the SQUID is providing the necessary transimpedance gain for the TES current to suppress the noise of preamplifier. In order to keep the output of SQUID in a small linear regime, the readout circuit employs a flux-locked loop (FLL)[25] in which the feedback current is inductively coupled to the SQUID through a feedback resistor $R_{\rm fb}$.

The TES coupled to the SQUID has been proven to show excellent single-pixel performance. However, for TES arrays, it is difficult to have a readout line for each pixel because each readout line brings a thermal load to the measurement system. In this case, SQUID-based multiplexing technologies, which can dramatically reduce the number of readout lines, are necessary for the readout of large-scale TES arrays.

In SQUID-based multiplexing technologies, different orthogonal modulation functions are used to encode and decode the TES signals.[26–28] In TDM, the functions are N low-duty-cycle square waves. In CDM, the functions correspond to an N-dimensional Walsh matrix in which N must be a power of two. In FDM, the functions correspond to N sinusoids which modulate TES signals to different frequencies. The functions of MW-Mux are similar to that of FDM. Therefore, the significant difference among these multiplexing technologies is the schemes used to combine and distinguish TES signals from different channels. These schemes are divided into time domain and frequency domain. In the following, this paper details these multiplexing schemes in the sequence of TDM, CDM, FDM and MW-Mux.

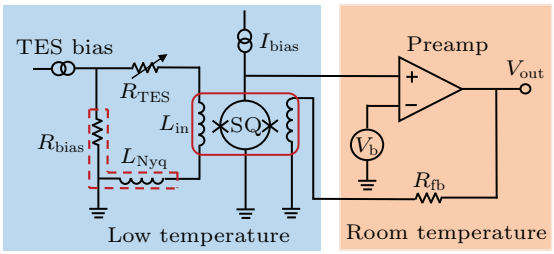


Fig. 1. Schematic of the readout circuit of a single TES. The SQUID chip (red solid box) generally consists of a SQUID amplifier, an input coil and a feedback coil. The Nyquist chip (red dotted box) generally consists of a bias resistor and a Nyquist coil.

3. Time-division multiplexing

At present, TDM is well-established for the readout of TES arrays. In the TDM circuit, each TES is equipped with a SQUID amplifier, which together constitute a pixel. In an individual column, TDM turns on each row of SQUIDs sequentially and combines the signals from different pixels into a common readout line.

3.1. TDM circuit architecture based on flux summing

The mature version of TDM circuits is based on an architecture which utilizes an approach of flux summing.[29] Figure 2 shows the schematic of this version. In each unit pixel, the TES is inductively coupled to a first-stage SQUID amplifier (SQ1). All the TESs operate in voltage-biased mode and remain active all the time. The SQ1 of each row is turned on by applying the row-address current ($I_{\rm ad}$) to the corresponding row-address line. Then, the current signal from SQ1 at a time is passed to a common second-stage SQUID (SQ2) via an intermediate summing coil. Next, the current signal from SQ2 is amplified by a third-stage SQUID array which is connected to room-temperature electronics. The entire TDM circuit uses a flux-locked loop (FLL) to keep the output signal of SQUID arrays within a small linear range. Each column in the circuit shares a feedback line through which a

proportional-integral feedback signal ($V_{\rm fb}$) is inductively coupled to SQ1s. The FLL is either traditional analog integrator circuits[30] or digital feedback control circuits (DFB).[31,32] This version of TDM circuits has been fielded in a variety of x-ray spectrometers.[33–35] The circuit architecture in Fig. 2 is a three-stage SQUID configuration. Actually, the architecture can be either two-stage or three-stage, as long as the configuration provides sufficient power gain for TES signals.

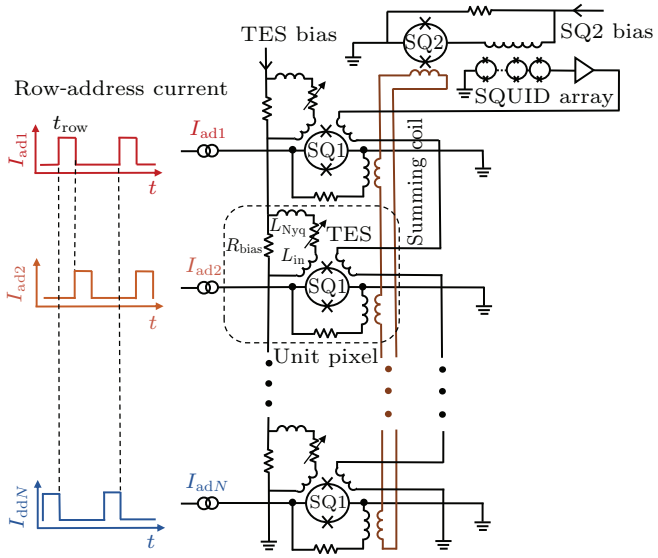


Fig. 2. Schematic of an N-row TDM circuit. The figure is taken from Ref. [29].

3.2. TDM circuit architecture based on superconducting switch

The TDM circuit above has a complex layout, and its row switching rate is not high enough. After iterative upgrades, TDM circuits have evolved into some new versions.[36–38] Compared with TDM circuits based on the flux summing, these versions remove the intermediate summing coil and introduce additional superconducting switches actuated by magnetic flux. Figure 3 shows the schematic of an N-row TDM circuit based on the flux-actuated superconducting switch. In each unit pixel, the superconducting switch (marked by a red dotted box) is in parallel with an input SQUID (SQ1 or SQ2$\cdots$SQN) and an addressing resistor $R_{\rm add}$. The addressing resistor is used to dissipate the weak loop current and its resistance needs to be smaller than the SQUID dynamic resistance to reduce its voltage noise. These superconducting switches are shorted in the non-address state. When a row-address current is applied to one switch, the switch is turned on while the others in the column are left shorted. In this situation, the signal from one SQUID is measured only once in one cycle of the row-address current. Compared with TDM circuits based on the flux summing, TDM circuits based on the superconducting switch have faster row switching rate and lower readout noise.

One form of the superconducting switch is the Zappe-style interferometer.[39] It includes tow-junction, three-junction and even multiple-junction configurations. In these configurations, Josephson junctions are connected in parallel by superconducting inductors and the feed point of the bias current is flexible. The bias current of the Zappe-style interferometer is set to be smaller than the critical current of the Josephson junction. Under this condition, the interferometer is in the zero-voltage state and the load of the interferometer is effectively shorted. When the critical current is reduced below the bias current by the external control current, nearly all the junction current flows into the load. The threshold curve of the Zappe-style interferometer can be adjusted by the critical current of the Josephson junction, the inductance and the feed point of the bias current, making the Zappe-style interferometer adaptable to different applications.

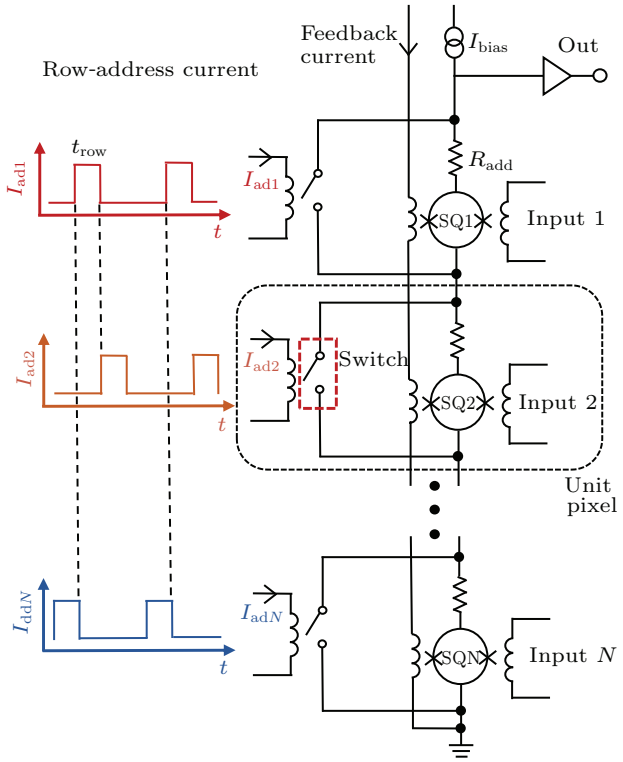


Fig. 3. Schematic of a TDM circuit with flux-actuated superconducting switches. The figure is taken from Ref. [36].

Another form of the superconducting switch is the SQUID-based switch.[36] The switch is essentially a SQUID with the extremely small loop inductance. In this SQUID, the screening parameter ($\beta_{\rm L} \ll 1$) is so small that the critical current of the SQUID approaches to zero at half-integer flux quanta. Similarly, the hysteresis parameter $\beta_{\rm C}$ needs to be sufficiently small to ensure that the current-voltage characteristics of this SQUID is non-hysteresis. The operation of the SQUID-based superconducting switch is as follows. The bias current ($I_{\rm bias}$) of the entire loop is selected to be not only slightly larger than the current ($I_{\rm sq}$) used to bias the input SQUID, but also smaller than the critical current ($I_{\rm c}$) of the SQUID-based switch at integer flux quanta. When the flux through the switch

is of integer flux quanta, the switch is in the superconducting state and the input SQUID is shorted. When a current that generates a flux of half-integer flux quanta is applied to the row-address line, the switch is in the resistive state and most of $I_{\rm bias}$ flows into the input SQUID. As long as circuit parameters are designed properly, the current flowing into the input SQUID can be equal to $I_{\rm sq}$ used to activate the input SQUID. The SQUID-based switch is generally in the form of a SQUID series array (SSA) to minimize loading of the activated input SQUID. The input SQUID can be either a single one or an array. An array configuration is preferable because it can improve the noise impedance match between SQUIDs and room temperature electronics.[40–42]

In the TDM circuit with superconducting switches discussed above, the number of row-address lines (used to turn on rows of SQUIDs) increases with the increase of the multiplexing factor, adding the burden of wiring. In order to alleviate the burden, an advanced two-level switch is proposed.[43] Figure 4 shows a simple example of the two-level switch. N superconducting switches are divided into N_1 groups (the first level), and each group contains N_2 switches (the second level), i.e., $N = N_1 \times N_2$. In this new architecture, the number of row-address lines reduces from $N_1 \times N_2$ to $N_1 + N_2$. This advantage becomes significant when the scale of TES arrays expands. However, extending the switches to multi-level structure complicates the design of cryogenic chips and room-temperature electronics.

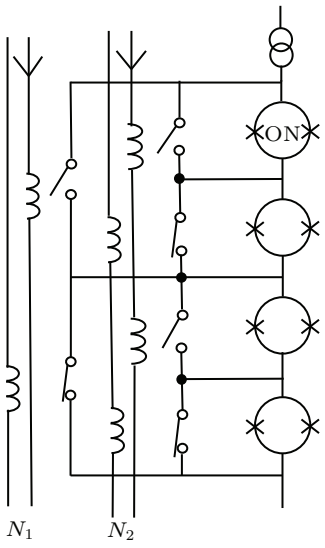


Fig. 4. The simple two-level switch layout. The figure is taken from Ref. [43].

3.3. Parameter constraints in TDM

In practical applications, TDM has its own parameter constraints. On the one hand, TDM imposes strict requirements on the sampling frequency. When rows of a TDM circuit are turned on sequentially, the row time which dwells on a row is denoted as $\delta t_{\rm row}$. For an N-row TDM circuit, the frame rate at which all the pixels in each column are measured can be expressed as $f_{\rm frame} = 1/(N\delta t_{\rm row})$. According to the Nyquist–Shannon theorem, the frame rate needs to satisfy the following condition to prevent high-frequency noise from aliasing into the signal bandwidth:

$$f_{\rm frame} > 2f_{\rm L/R}, \tag{1}$$

where $f_{\rm L/R}$ is the cut-off frequency of the L/R low-pass filter in the TES bias circuit. The inductance L is the sum of the input inductance, the Nyquist inductance and the stray inductance. The resistance R is the total resistance in the TES bias circuit. Meanwhile, the TES under electrothermal negative feedback (ETF) should satisfy the following condition[44] to ensure the stability of the device:

$$f_{\rm L/R} > \left(3+2\sqrt{2}\right) f_{\rm TES}, \tag{2}$$

where $f_{\rm TES}$ is the thermal response frequency of the TES. The sampling frequency $f_{\rm sample}$, which denotes as the switching rate between adjacent rows, is N times the frame rate. Combining the conditions above, the sampling frequency is limited to the following condition:

$$f_{\rm sample} > 2N\left(3+2\sqrt{2}\right) f_{\rm TES}. \tag{3}$$

It can be seen that TDM requires an extremely high sampling frequency when it is used to read out fast photon signals or a large number of pixels. In addition, when the TDM circuit switches from one row to the next, SQUIDs require a settling time to establish a stable state due to the transient response of the electronic components.[45] As a result, the time that can be used to sample is even shorter than the row time, presenting an additional challenge to the sampling frequency. Although an extra inductor in series with TES can limit the signal bandwidth and thus reduce the settling time, it comes at the expense of the reduction of signal-to-noise ratio (SNR).

One the other hand, the multiplexing factor of TDM is largely limited by the SQUID noise. The TES in the TDM circuit operates at all times while SQUIDs of each row only operate in a cycle of $1/N$. In this case, the effective bandwidth of the SQUID noise is N times larger than that of the TES noise, resulting in the input-referred current noise of the SQUID increasing by $\sqrt{N}$. This is generally referred to as the $\sqrt{N}$ noise penalty in TDM. Therefore, a large N may not be appropriate for TDM because the input-referred current noise of the SQUID needs to be smaller than the current noise of a single TES to prevent TES signals from being annihilated. Although the input-referred current noise of SQUID can be reduced by increasing the mutual inductance between the input coil and the SQUID, the signal slew rate is also increased. An increased signal slew rate is difficult for the TDM circuit to establish the FLL,[46] causing the degradation of TES signals.

As a mature multiplexing technology, TDM has been widely used for the readout of arrays of microcalorimeters and bolometers. When TDM is applied to TES microcalorimeters, a TDM circuit based on the superconducting switch, with 160 ns row times and the equivalent flux noise of 0.19 $\mu\Phi_0/\sqrt{\text{Hz}}$, achieves 2.55 eV resolution in a 32-row array of x-ray TESs.[38] In addition, the readout of a TES array with 256 gamma-ray TESs is demonstrated, showing energy resolution of 53 eV at 97 keV.[47] For the measurement of the B-mode polarization of CMB, a TDM system achieves a multiplexing factor of 128 in the array of TES bolometers.[48] Due to the simplicity in operation and the maturity in circuit architectures, TDM is considered to be suitable for the multiplexed readout of different TES arrays.

4. Code-division multiplexing

CDM is another scheme in the time domain, which has great potential for the readout of large arrays of TESs or fast pixels. In the implementation of CDM, the signals from TES detectors are coupled to the SQUIDs through different polarity combinations which correspond to the Walsh matrix. The original TES signals can be reconstructed from the raw output by the inversion of Walsh matrix. Like TDM, CDM rows are turned on by applying row-address current. The difference between them is that TDM rows are sampled only once in each frame while CDM rows are sampled at all times.[49] In this case, the signal-to-noise ratio of CDM increases by $\sqrt{N}$, compensating for the degradation of $\sqrt{N}$ SQUID noise. Unlike TDM, CDM does not suffer from the $\sqrt{N}$ noise penalty. Therefore, CDM does not require so large mutual inductance between the input coil and the SQUID as TDM to suppress the effective SQUID noise, relaxing the requirements for the dynamic range of the SQUID. At present, there are two approaches to CDM, namely flux summation (Φ-CDM) and current steering (I-CDM), which are based on different mechanisms.

4.1. Flux-summation architecture

Φ-CDM achieves different coupling polarities between the signal and the SQUID by changing the direction of the input coil in the TES bias circuit.[50] Figure 5 shows a schematic of a four-row Φ-CDM circuit which is based on a three-stage SQUID architecture. In the Φ-CDM circuit, the polarity combination of each row used to encode TES signals corresponds to the Walsh function. As with TDM, each row of the Φ-CDM circuit is turned on by applying row-address currents in sequence. TES signals with different polarity combinations are coupled to the first-stage SQUIDs (SQ1). Next, the signals from different rows are passed to a common SQUID amplifier (SQ2) through an inductive coil. The signals from SQ2 are amplified by a SQUID array and transmitted to room-temperature electronics for demodulation. The original TES signals can be demodulated and identified according to the inversion of Walsh matrix. When any SQUID in the circuit is taken for observation, all the TESs are connected to this SQUID. The SQUID noise in CDM can be improved because the SQUID in each row observes the Walsh-coded TES signals simultaneously. Φ-CDM is developed straightly based on TDM and shares similar low-pass filters with it.

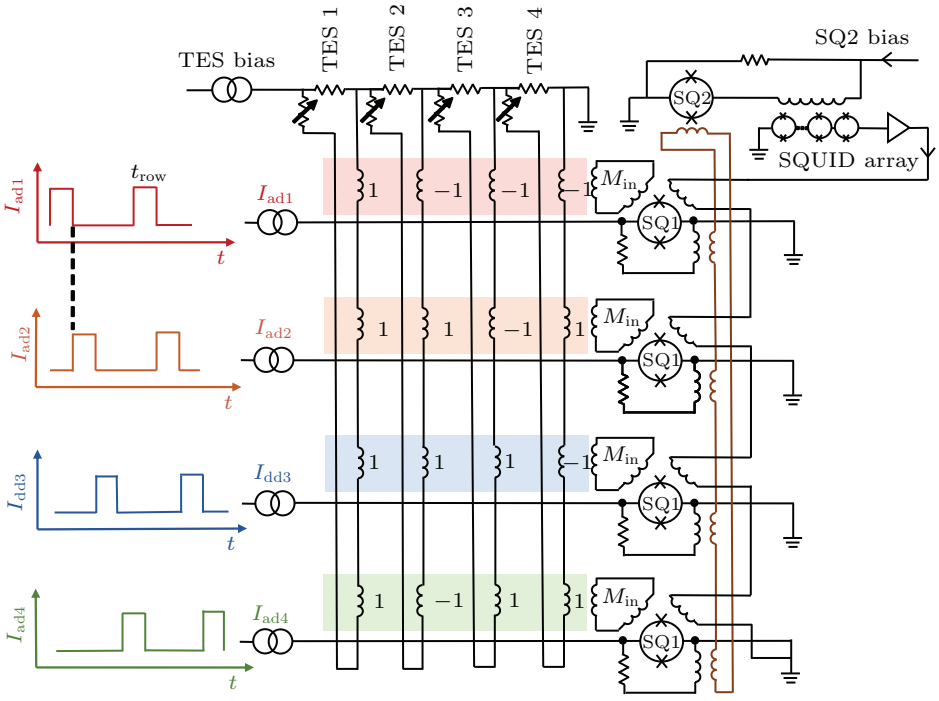


Fig. 5. Schematic of a four-row Φ-CDM. The figure is taken from Ref. [50].

4.2. Current-steering architecture

In *I*-CDM, the polarity switching of TES signals is realized through a single-pole double-throw (SPDT) switch.[51] Figure 6 shows the schematic of a four-row *I*-CDM circuit and an SPDT switch integrated with a TES bias circuit. The SPDT switch consists of two SQUID-based switches connected in parallel. Each branch contains a SQUID-based switch (actually a DC-SQUID with the extremely small loop inductance), a series resistor $R_{\rm ser}$, and an inductive coil coupled to the summing coil. The coupling polarity between one branch and the summing coil is positive (mutual inductance $+M$) while the other is negative (mutual inductance $-M$). The critical current of the DC-SQUID with the extremely small loop inductance approaches zero at half-integer flux quanta. In the implementation of *I*-CDM, a flux offset of $\Phi_0/2$ is applied to one of the SQUID-based switches in the SPDT to make the critical current of that switch reduce to a minimum. In this case, one SQUID-based switch becomes resistive state ($R_{\rm N}$) while the other keeps superconducting state. Since the normal resistance of the SQUID-based switch is much larger than the series resistance, i.e., $R_{\rm N} \gg R_{\rm ser}$, almost all of the TES current flows through the superconducting SQUID-based switch. The coupling polarity between the TES signal and the summing coil can be adjusted by applying row-address currents to generate 0 or $\Phi_0/2$ flux in the entire SPDT switch. The row-address currents in *I*-CDM correspond to the Walsh matrix. The difference between row-address currents in Φ-CDM and *I*-CDM is that currents in Φ-CDM are applied sequentially to rows in a cycle while currents in *I*-CDM are simultaneously applied to rows.

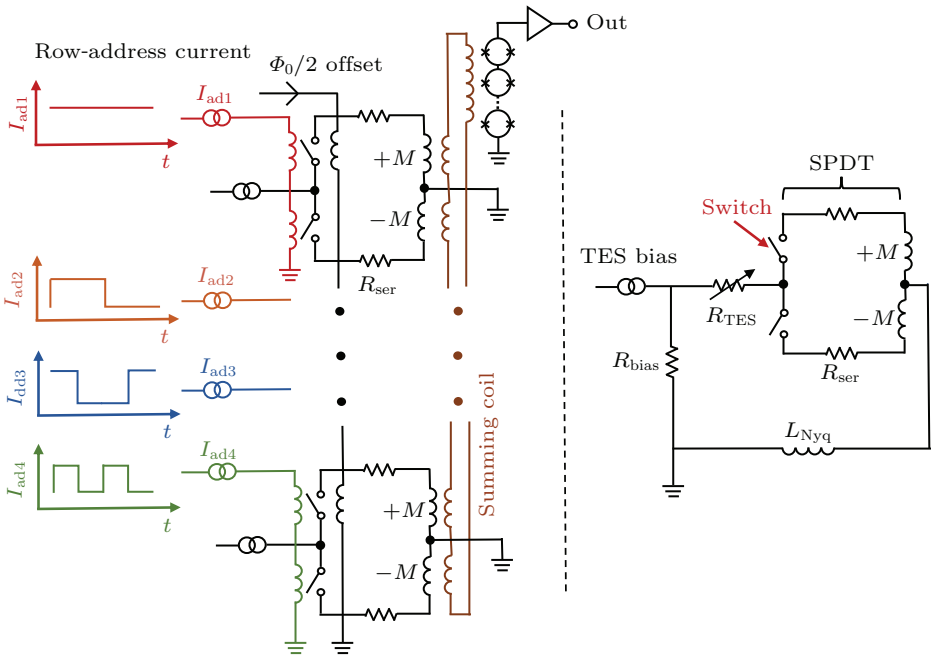


Fig. 6. Schematic of a four-row *I*-CDM circuit and an SPDT switch integrated with a TES bias circuit. The figure is taken from Ref. [51].

4.3. Parameter constraints in CDM

Each CDM approach has its own parameter constraints. In Φ-CDM, TESs are inductively coupled to the SQUID in different rows through different polarity combinations. Since the input coil of each TES needs to be routed to all the first-stage input SQUIDs, the large routing length presents a great challenge to the fabrication process. In *I*-CDM, the coupling polarity is modulated by an SPDT switch placed in the TES bias circuit. However, the resistive SQUID-based switch appears as an additional load resistance in series with the TES, interfering the measured TES current. In addition, the voltage across the resistive SQUID-based switch can easily induce the Josephson oscillation at the frequency of V/Φ_0.[49]

Both CDM approaches also have some constraints in common. Firstly, the coupling polarity in the first channel of CDM is always positive, which easily induces large crosstalk from feedback signals of other channels.[51] In practical applications, the first channel is usually used to characterize common coherent noise sources and the rest are used to read out TES detectors. Secondly, CDM is vulnerable to the signal loss. Since each SQUID in a column is a necessary component to obtain the encoded TES signal, a failed SQUID can result in the loss of an entire column of TES signals. To solve this problem, an error correction (EC) which replaces one TES with a constant signal is used to recover TES signals in the case of a failed SQUID.[52] A configurable error correction integrated with a cryotron switch in the TES bias circuit is also demonstrated.[53] In room-temperature electronics of CDM, a complex set of algorithm software is required to perform the

Walsh encoding. Meanwhile, the channel crosstalk caused by parallel readout needs to be optimized.[54]

Despite the constraints above, CDM has some distinctive advantages. Since every TES in CDM is sampled during every switching cycle, information about photon arrival time can be obtained from the modulated data stream.[49,51] In addition, using the periodic characteristics of SQUID response, binary addressing is expected to reduce the number of row-address lines from N to $\log_2 N$.[55] Since CDM does not suffer from the $\sqrt{N}$ noise penalty, CDM has potential for the readout of fast signals. In some demonstrations of small-scale TES arrays, the readout noise of a Φ-CDM circuit used to read out x-ray TESs is about 19 pA/$\sqrt{\text{Hz}}$ at high frequencies[50] and an I-CDM circuit is not degraded by the $\sqrt{N}$ SQUID noise penalty.[51] With the development of CDM technology, Φ-CDM stretches to a 32-channel circuit in which 30 modulated TESs achieve 2.77 eV energy resolution at 5.9 keV.[56] In addition, some hybrid readout schemes, which combine CDM with other multiplexing schemes, are expected to increase the multiplexing factor and to improve the circuit performance.[57–59]

5. Frequency-division multiplexing

FDM combines and distinguishes signals from different channels in the frequency domain, which is an attractive technology for the readout of TES arrays and has some different characteristics.

5.1. FDM circuit architecture

In the implementation of FDM at MHz frequencies, the TES detector is ac-biased.[60,61] Figure 7 shows the schematic of an N-channel FDM circuit. In each unit pixel, the TES resistance R_{TES} is connected with an inductor L and a capacitor C to form an LCR filter on the sub-Kelvin stage. The TES resistance and the inductor in all channels are the same while the capacitor is different from each other. In each channel, the bandwidth for the TES detector is expressed as $R/2\pi L$ and the resonant frequency of the LCR filter is determined by the value of the capacitance. Bias carriers with different frequencies are applied to TES bias circuits and thus TES signals are modulated to high frequencies. The LCR filter of each channel is used to pass through the target carrier frequency and suppress out-of-band signals and noise. When the TES resistance R_{TES} changes, the corresponding carrier is amplitude modulated and the TES signal is encoded in sidebands above and below the carrier. These encoded TES signals from different channels are coupled to a common SQUID amplifier (typically a SQUID array) on the Kelvin stage. Then output signals of the SQUID are passed to room-temperature electronics for demodulation.

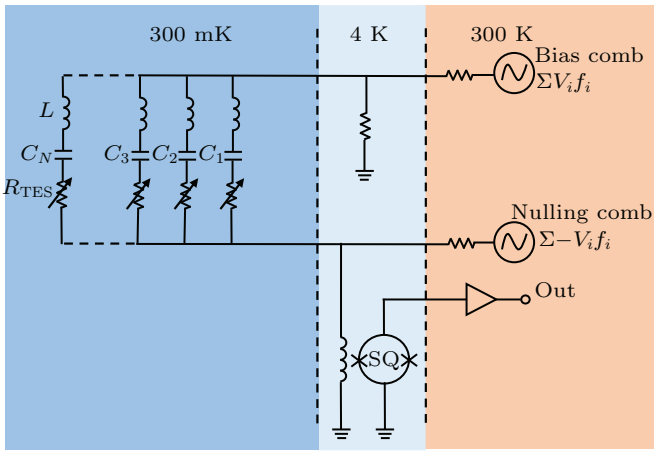


Fig. 7. Schematic of an N-channel FDM circuit. The figure is taken from Ref. [61].

Since signals from individual channels are coupled to a common SQUID amplifier, the dynamic range of the SQUID that can accommodate the carrier signals is limited. In order to extend the dynamic range of the SQUID, a carrier comb with a phase shift of π, which is referred to as the nulling comb, is injected at the input of the SQUID to cancel the carrier signals applied to TESs.[62] Another effective way to this problem is feedback. Some studies have shown that baseband feedback (BBFB)[63] or digital active nulling (DAN)[64] can increase the dynamic range of the SQUID, allowing an increased number of TES detectors per readout SQUID. The complexity of code for BBFB is comparable to the code for frame-delayed flux feedback used in TDM, which is important for practical applications of FDM. The improvement to the dynamic range of the SQUID can also be reached by increasing the number of SQUIDs for readout within a dissipation budget constraint.

5.2. Parameter constraints in FDM

Since the bandwidth of the SQUID amplifier can be limited to the same bandwidth as the TES, FDM does not suffer from the $\sqrt{N}$ noise penalty.[65] In addition, TES signals in FDM are generally modulated to high frequencies, avoiding the effect of low frequency noise.

However, FDM has its own problems. Firstly, compared with the dc-biased TES in TDM and CDM, the ac-biased TES in FDM shows resolution degradation.[66,67] Secondly, the size of filter elements in FDM is slightly larger than that in TDM and CDM. The inductor in FDM is effectively same as the Nyquist inductor in TDM or CDM, and the capacitor in the optimally dimensioned circuit is approximately the same size as the inductor.[68] In an optimal case, the size of filter elements of FDM is twice that of TDM or CDM.[69] Thirdly, the crosstalk effect in FDM circuits makes it difficult to accurately demodulate carriers and identify TES signals in room-temperature electronics. It has been suggested that one of the reasons for the crosstalk effect is due to the nonlinearity of the SQUID response.[70] Some other contributions to

channel-to-channel crosstalk include the coupling between inductors of different channels, bias carrier leakage and non-zero SQUID/wiring impedance.[71] In order to prevent channel crosstalk, the frequency space between adjacent resonances needs to be sufficiently separated.[72,73]

In the demonstration of the readout of x-ray microcalorimeters, an FDM circuit based on BBFB can multiplex 16 TES detectors with a sufficient post-demodulation gain-bandwidth product and SNR.[63] As the readout system continues to develop, the dynamic range of the SQUID is greatly increased, extending the number of TES microcalorimeters per readout SQUID in the FDM circuit to 40.[74] FDM is also widely used in readout circuits of TES bolometers. As for a 64-pixel bolometric setup, the noise level of its FDM circuit is about 10 pA/$\sqrt{\text{Hz}}$.[75] With the development of FDM, the number of TES bolometers in each readout channel reaches about 160.[76]

6. Microwave SQUID multiplexing

Another technology for reading out signals in the frequency domain is MW-Mux. Because MW-Mux can provide hundreds of MHz or even several GHz bandwidths for the whole readout circuit, it attracts extensive attention in recent years.

6.1. MW-Mux circuit architecture

MW-Mux retains the key attribute of dc-biased TES detectors as with TDM and CDM. Figure 8 shows the schematic of a microwave SQUID multiplexing circuit. In the MW-Mux circuit, each TES is coupled to an intermediate SQUID. The SQUID can be either a DC-SQUID[77] or a dissipationless RF-SQUID.[78–80] Each SQUID is coupled to a high-Q microwave resonator which has a unique resonant frequency. The TES current is inductively coupled to the SQUID and generates a flux in the SQUID. The change of the flux results in a change in the Josephson inductance of the SQUID, causing a shift in the resonant frequency of the corresponding resonator. The microwave SQUID multiplexer contains many resonators which are all coupled to a common coplanar waveguide (CPW) readout line. The frequency shifts induced by TES signals are probed by applying a comb of microwave signals to the CPW readout line.[81] The probed signals are amplified by a high-electron-mobility transistor (HEMT) amplifier at 4 K and then passed to room-temperature electronics for demodulation.

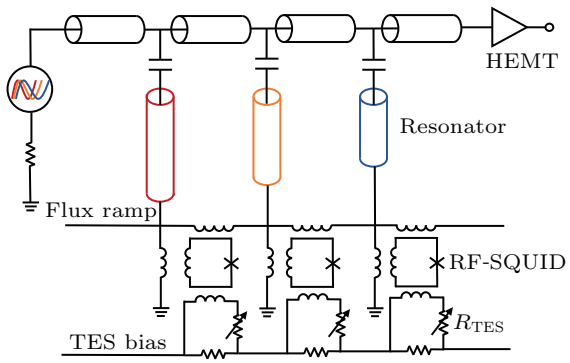


Fig. 8. Schematic of a three-pixel microwave SQUID multiplexing circuit. The figure is taken from Ref. [81].

6.2. Flux ramp modulation

Since the flux-voltage characteristics of the SQUID is periodic, the feedback loop is required to keep the response of the SQUID in a linear range and to bias the flux at a sensitive point of the SQUID response curve. Typically, TDM, CDM and FDM are all configured with feedback loops. Nevertheless, the flux-locked loop seems not to be compatible with MW-Mux. An alternative approach for MW-Mux is flux ramp modulation.[82] When a periodic sawtooth-shaped current signal is applied to a common modulation coil and generates a linearly rising flux ramp of an integer flux quanta in the SQUID, the SQUID response changes according to its flux-voltage characteristics. The flux ramp repetition rate f_{ramp} corresponds to the effective sampling frequency of TES signals. When f_{ramp} is larger than the slew rate of the input signal, the phase shift of the flux-voltage characteristics is a linear function of the amplitude of the input signal. A change of one flux quantum corresponds to a phase shift of 2π. The phase shift can be determined by using software-defined radio (SDR)-based readout electronics.[83]

Flux ramp modulation can not only provide a linear measurement for the input signal, but also increase the usable dynamic range of the SQUID. In practical applications, different types of TES detectors have different requirements on f_{ramp} and the bandwidth of the resonator is adjusted according to f_{ramp}. The bandwidth of the resonator can be set by adjusting the strength of the capacitive coupling between the resonator and the CPW readout line.

6.3. Parameter constraints in MW-Mux

The significant advantage of MW-Mux is the large readout bandwidth. The large readout bandwidth enables MW-Mux to measure a large number of TES detectors simultaneously. Alternatively, MW-Mux can allocate sufficient bandwidth for each pixel, which is suitable for the readout of TES detectors with rapid signal rate and high bandwidth requirements. In practical applications of MW-Mux, the number of TES detectors in each readout channel (the multiplexing factor) is limited by the allowable resonance spacing and the available bandwidth of room-temperature electronics.

Firstly, the sufficient resonance spacing in MW-Mux is required to reduce channel-to-channel crosstalk because the overlapping tails of Lorentzian resonance profiles have influ-

ence on the sensitivity of the entire readout system. The resonance spacing is associated with allowable level of crosstalk and the input signal slew rate. In general, when resonance spacing is roughly 10 times the bandwidth of the resonator, the channel crosstalk can be kept below 0.1%.[84,85] Secondly, the readout bandwidth of MW-Mux is typically limited to 4–8 GHz, but practical readout bandwidth of the entire system is determined by the room-temperature electronics. For probing the phase shift of resonant frequencies, the control electronics generate the tones at baseband and mix them up to microwave frequencies. For flux ramp demodulation, the readout electronics adopt a software-defined algorithm to identify the phase shift of the SQUID response. With the significant increase in the number of TES detectors in each readout channel, it is challengeable for room-temperature electronics to generate and demodulate such a large number of microwave signals to satisfy the readout requirements of large-scale TES arrays.[86] Room-temperature electronics of MW-Mux are being developed and optimized to expand the total readout bandwidth.

The first demonstration of MW-Mux showed that the equivalent flux noise was about 0.5 $\mu\Phi_0/\sqrt{\text{Hz}}$.[87] To date, there are many applications based on MW-Mux. In the demonstration of the readout of γ-ray TES microcalorimeters, MW-Mux achieves a multiplexing factor of 128 and a sampling frequency of 62.5 kHz.[88] When MW-Mux is used to read out 38 x-ray TESs simultaneously, it achieves a sampling frequency of 500 kHz and an excellent noise level of 9 pA/$\sqrt{\text{Hz}}$.[89] Since MW-Mux can provide sufficient bandwidth for each TES detector in which the signal switching rate is rapid, it is also considered to be suitable for the readout of optical TES arrays.[90] As for the readout of arrays of TES bolometers, MW-Mux is used to construct a 1820-channel multiplexer within a 4–8 GHz readout band.[91]

7. Characteristics of different multiplexing technologies

SQUID-based multiplexing technologies make the readout of large-scale TES arrays feasible. In order to advance SQUID-based multiplexing technologies over a wide frequency range, optimization and improvement for the entire readout system are required. Since each technology has its own advantages and disadvantages, finding a balance among its characteristics to realize a high-performance readout system is an important topic. Table 1 compares characteristics of different multiplexing technologies. When one multiplexing technology is applied to TES microcalorimeters and TES bolometers separately, the multiplexing factors of the two devices are different. Since TES microcalorimeters are used to detect x rays and gamma rays, and TES bolometers are used to detect sub-mm and microwave signals, they have different requirements for the pixel bandwidth. In general, TES microcalorimeters require larger pixel bandwidth than TES bolometers, which imposes restrictions on the multiplexing factor of TES microcalorimeters in the case that the total bandwidth of the readout system is limited. In Table 1, the multiplexing factors of TES microcalorimeters and TES bolometers are separately stated and the readout noise corresponds to the noise level achieved at the same multiplexing factor. The development goals of multiplexing technologies are to achieve large multiplexing factor while ensuring low readout noise of the entire system. Besides the multiplexing factor and the readout noise, some other characteristics such as the crosstalk, the chip area occupied by the filter element and the complexity of room-temperature electronics, also need to be taken into account in practical applications.

TDM is competitive in the characterization and the readout of small-scale TES arrays because of its simplicity. Nevertheless, due to the slow row switching rate and the $\sqrt{N}$ noise penalty, TDM is difficult to achieve a large multiplexing factor, especially for the multiplexed readout of fast photon signals. CDM adopts the Walsh matrix to encode TES signals, which is promising in improving the circuit performance and enhancing the scalability of TES arrays. However, the Walsh encoding also brings complex designs to CDM circuits. FDM modulates TES signals to high frequencies to reduce the effect of low-frequency noise, but the ac bias of the TES detector places an inherent constraint on FDM circuits. MW-Mux is expected to significantly increase the scale of TES arrays and read out fast photon signals due to the large readout bandwidth. Although MW-Mux is promising in the scalable readout, much work needs to be carried out on its room-temperature electronics. As for TES arrays with different types and different pixel numbers, selecting an appropriate multiplexing scheme enables the entire readout system to achieve an optimized performance.

Table 1. Characteristics of different multiplexing technologies.

Multiplexing scheme	Multiplexing factor		Readout noise[a] ($\mu\Phi_0/\sqrt{\text{Hz}}$)		Room-temperature electronics
	Calorimeter	Bolometer	Calorimeter	Bolometer	
TDM	32[38]	128[48]	0.19[38]	–	Frame-delayed flux feedback[38]
CDM	32[56]	–	0.17[56]	–	Walsh coding[49]
FDM	40[74]	$\sim$ 160[76]	0.18[74]	0.2[76]	Baseband feedback[63]
MW-Mux	128[88]	$\sim$ 1820[91]	2.0[88]	4.5[91]	Flux ramp modulation[82]

[a]The readout noise is usually denoted as the non-multiplexed flux noise of the entire readout system and referred to the first-stage SQUID.

8. Summary

SQUID-based multiplexing technologies are compatible with a variety of cryogenic applications. This paper focuses on the multiplexed readout of TES arrays and reviews different types of multiplexing technologies including TDM, CDM, FDM and MW-Mux. Overall, SQUID-based multiplexing technologies are necessary for the readout of TES arrays. New applications that require large-scale TES arrays emphasize the importance of developing multiplexing technologies with large multiplexing factors and low readout noise. As advances continue in circuit architectures, room-temperature control and readout systems, SQUID-based multiplexing technologies are expected to meet the demands of future arrays of TES detectors.

Acknowledgements

Project supported by the National Science Foundation of China (Grant Nos. 11653001 and 11653004). The authors thank Changhao Zhao, Rutian Huang, Kaiyong He, Xiao Geng, Genting Dai and Liangliang Yang for valuable discussions.

References

[1] Ullom J N, Beall J A, Doriese W B, Duncan W D, Ferreira L, Hilton G C, Irwin K D, Reintsema C D and Vale L R 2005 *Appl. Phys. Lett.* **87** 194103
[2] Oshima T, Yamakawa Y, Kurabayashi H, Hoshino A, Ishisaki Y, Ohashi T, Mitsuda K and Tanaka K 2008 *J. Low Temp. Phys.* **151** 430
[3] Miyazaki T, Ullom J N, Cunningham M F and Labov S E 2003 *IEEE Trans. Appl. Supercond.* **13** 630
[4] Ezoe Y, Ohashi T and Mitsuda K 2021 *Rev. Mod. Plasma Phys.* **5** 4
[5] Zhang H J, Wen J, Mo Z H, Liu H R, Wang X D, Xiong Z H, Zhang J W and Shuai M B 2021 *Chin. Phys. B* **30** 117401
[6] Bonetti J A, Turner A D, Bock J J, Brevik J A, Day P K, Filippini J, Golwala S R, Holmes W, Jones W C and Kenyon M 2012 *J. Low Temp. Phys.* **167** 146
[7] Suzuki T, Khosropanah P, Hijmering R A, Ridder M, Schoemans M, Hoevers H and Gao J R 2014 *IEEE Trans. Terahertz Sci. Technol.* **4** 171
[8] Marnieros S, Ade P, Alberro J G, Almela A and Zullo A 2020 *J. Low Temp. Phys.* **199** 955
[9] O'Brient R, Ade P, Arnold K, Edwards J, Engargiola G, Holzapfel W L, Lee A T, Myers M J, Quealy E, Rebeiz G, Richards P and Suzuki A 2013 *Appl. Phys. Lett.* **102** 063506
[10] Karasik B S and Cantor R 2011 *Appl. Phys. Lett.* **98** 193503
[11] Lolli L, Taralli E, Portesi C, Monticone E and Rajteri M 2013 *Appl. Phys. Lett.* **103** 041107
[12] Lolli L, Taralli E, Rajteri M 2012 *J. Low Temp. Phys.* **167** 803
[13] Lolli L, Taralli E, Portesi C, Rajteri M and Monticone E 2016 *Sensors* **16** 953
[14] Schmidt M, von Helversen M, López M, Gericke F, Schlottmann E, Heindel T, Kück S, Reitzenstein S and Beyer J 2018 *J. Low Temp. Phys.* **193** 1243
[15] Zhang Q Y, Wang T S, Liu J S, Dong W H, He G F, Li T F, Zhou X X and C W 2014 *Chin. Phys. B* **23** 118502
[16] Braginski A I and Clarke J 2004 *The SQUID Handbook: Fundamentals and Technology of SQUIDs and SQUID Systems* (New York: Wiley) vol. I pp. 1–28
[17] Granata C, Russo C D, Monaco A and Russo M 2001 *IEEE Trans. Appl. Supercond.* **11** 95
[18] Shimizu N, Chiba N, Yabe S, Ishikawa T, Chinone K and Kiryu S 1993 *IEEE Trans. Appl. Supercond.* **3** 1828
[19] Irwin K D, Hilton G C, Martinis J M and Cabrera B 1996 *Nucl. Instrum. Methods Phys. Res. A* **370** 177
[20] Luukanen A, Kinnunen K M, Nuottajärvi A K, Hoevers H F C, Bergmann Tiest W M and Pekola J P 2003 *Phys. Rev. Lett.* **90** 238306
[21] Mo Z H, Lu C, Liu Y, Feng W, Zhang Y, Zhang W, Tan S Y, Zhang H J, Guo C Y, Wang X D, Wang L, Yang R Z, Ren Z G, Zhu X G, Xiong Z H, An Q and Lai X C 2018 *Chin. Phys. B* **27** 067403
[22] Morgan K M, Pappas C G, Bennett D A, Gard J D, Hays-Wehle J P, Hilton G C, Reintsema C D, Schmidt D R, Ullom J N and Swetz D S 2017 *Appl. Phys. Lett.* **110** 212602
[23] Irwin K D 1995 *Appl. Phys. Lett.* **66** 1998
[24] Lee S F, Gildemeister J M, Holmes W, Lee A T and Richards P L 1998 *Appl. Opt.* **37** 3391
[25] Foglietti V, Stawiasz K G, Ketchen M B and Koch R H 1993 *IEEE Trans. Appl. Supercond.* **3** 3061
[26] Irwin K D and Hilton G C 2005 *Cryogenic Particle Detection* (Topics in Applied Physics) vol. 99 (Berlin: Springer) pp. 63–150
[27] Kiviranta M, Seppa H, Kuur J and Korte P 2002 *AIP Conf. Proc.* **605** 295
[28] Ullom J N and Bennett D A 2015 *Supercond. Sci. Technol.* **28** 084003
[29] Doriese W B, Ullom J N, Beall J A, Duncan W D, Ferreira L, Hilton G C, Horansky R D, Irwin K D, Mates J A B, Reintsema C D, Vale L R, Xu Y, Zink B L, Rabin M W, Hoover A S, Rudy C R and Vo D T 2007 *Appl. Phys. Lett.* **90** 193508
[30] Drung D 2002 *Physica C* **368** 134
[31] Myoren H, Goto M, Taino T, Kikuchi K, Nakagawa H, Tokoro K, Aoyagi M and Takada S 2005 *IEEE Trans. Appl. Supercond.* **15** 332
[32] Durkin M, O'Neil G C, Doriese W B, Gard J D, Hilton G C, Imrek J, Ortiz N, Reintsema C D, Stevens R W, Swetz D S and Ullom J N 2020 *J. Low Temp. Phys.* **199** 275
[33] Doriese W B, Beall J A, Deiker S, Duncan W D, Ferreira L, Hilton G C, Irwin K D, Reintsema C D, Ullom J N and Vale L R 2004 *Appl. Phys. Lett.* **85** 4762
[34] Uhlig J, Fullagar W, Ullim J N, Doriese W B, Fowler J W, Swetz D S, Gador N, Canton S E, Kinnunen K, Maasilta I J, Reintsema C D, Bennett D A, Vale L R, Hilton G C, Irwin K D, Schmidt D R and Sundström V 2013 *Phys. Rev. Lett.* **110** 138302
[35] Ullom J N, Doriese W B, Fischer D A, Fowler J W, Hilton G C, Jaye C, Reintsema C D, Swetz D S and Schmidt D R 2014 *Synchrotron Radiat. News* **27** 24
[36] Beyer J and Drung D 2008 *Supercond. Sci. Technol.* **21** 105022
[37] Beev N, Kiviranta M, van der Kuur J, Bruijn M, Brandel O, Linzen S, Fritzsch L, Ahoranta J, Penttilä J and Roschier L 2014 *J. Phys. Conf. Ser.* **507** 042003
[38] Doriese W B, Morgan K M, Bennett D A, Denison E V, Fitzgerald C P, Fowler J W, Gard J D, Hays-Wehle J P, Hilton G C, Irwin K D, Joe Y I, Mates J A B, O'Neil G C, Reintsema C D, Robbins N O, Schmidt D R, Swetz D S, Tatsuno H, Vale L R and Ullom J N 2016 *J. Low Temp. Phys.* **184** 389
[39] Zappe H H 1977 *IEEE Trans. Magn.* **13** 41
[40] Stawiasz K G and Ketchen M B 1993 *IEEE Trans. Appl. Supercond.* **3** 1808
[41] Morooka T, Tanaka K, Nagata A, Nakayama S and Chinone K 2003 *Physica B* **329–333** 1510
[42] Drung D, Aßmann C, Beyer J, Kirste A, Peters M, Ruede F and Schurig T 2007 *IEEE Trans. Appl. Supercond.* **17** 699
[43] Dawson C S, Chaudhuri S, Titus C J, Cho H-M, Denison E V, Doriese W B, Durkin M, FitzGerald C T, Hilton G C, Irwin K D, Li D, O'Neil G C, Reintsema C D, Steffen Z, Stevens R W, Swetz D S, Ullom J N, Vale L R, Weber J C and Young B A 2019 *IEEE Trans. Appl. Supercond.* **29** 2500205
[44] Irwin K D, Hilton G C, Wollman D A and Martinis J M 1998 *J. Appl. Phys.* **83** 3978
[45] Heinz E, Zakosarenko V, May T and Meyer H G 2013 *Supercond. Sci. Technol.* **26** 045013
[46] Drung D 2003 *Supercond. Sci. Technol.* **16** 1320
[47] Bennett D A, Horansky R D, Schmidt D R, Hoover A S, Winkler R, Alpert B K, Beall J A, Doriese W B, Fowler J W, Fitzgerald C P, Hilton G C, Irwin K D, Kotsubo V, Mates J A B, O'Neil G C, Rabin M W, Reintsema, Schima F J, Swetz D S, Vale L R and Ullom J N 2012 *Rev. Sci. Instrum.* **83** 093113

[48] Prêle D, Voisin F, Piat M, Decourcelle T, Perbost C, Chapron C, Rambaud D, Maestre S, Marty W and Montier L 2016 *J. Low Temp. Phys.* **184** 363

[49] Irwin K D, Niemack M D, Beyer J, Cho H M, Doriese W B, Hilton G C, Reintsema C D, Schmidt D R, Ullom J N and Vale L R 2010 *Supercond. Sci. Technol.* **23** 034004

[50] Stiehl G M, Doriese W B, Fowler J W, Hilton G C, Irwin K D, Reintsema C D, Schmidt D R, Swetz D S, Ullom J N and Vale L R 2012 *Appl. Phys. Lett.* **100** 072601

[51] Niemack M D, Beyer J, Cho H M, Doriese W B, Hilton G C, Irwin K D, Reintsema C D, Schmidt D R, Ullom J N and Vale L R 2010 *Appl. Phys. Lett.* **96** 163509

[52] Titus C J, Chaudhuri S, Cho H M, Dawson C, Doriese W B, Fowler J W, Hilton G C, Irwin K D, Kuenstner S, Li D, Morgan K, Reintsema C D, Swetz D S, Ullom J N and Young B A 2018 *J. Low Temp. Phys.* **193** 556

[53] Weber J C, Fowler J W, Durkin M, Morgan K M, Mates J A B, Bennett D A, Doriese W B, Schmidt D R, Hilton G C, Swetz D S and Ullom J N 2019 *Appl. Phys. Lett.* **114** 232602

[54] Fowler J W, Doriese W B, Hilton G, Irwin K, Schmidt D, Stiehl G, Swetz D, Ullom J N and Vale L 2012 *J. Low Temp. Phys.* **167** 713

[55] Irwin K D, Cho H M, Doriese W B, Fowler J W, Hilton G C, Niemack M D, Reintsema C D, Schmidt D R, Ullom J N and Vale L R 2012 *J. Low Temp. Phys.* **167** 588

[56] Morgan K M, Alpert B K, Bennett D A, Denison E V, Doriese W B, Fowler J W, Gard J D, Hilton G C, Irwin K D, Joe Y I, O'Neil G C, Reintsema C D, Schmidt D R, Ullom J N and Swetz D S 2016 *Appl. Phys. Lett.* **109** 112604

[57] Reintsema C D, Bennett D A, Denison E V, Durkin M, Doriese W B, Fowler J W, Gard J D, Grigorian A, Hilton G C, Hubmayr J, O'Neil G C, Mates J A B, Morgan K M, Schmidt D R, Stevens R W, Swetz D S, Vale L R, Ullom J N, Irwin K D, Chaudhuri S, Titus C J and Dawson C S 2019 *IEEE Trans. Appl. Supercond.* **29** 2500406

[58] Doriese W B, Bandler S R, Chaudhuri S, Dawson C S, Denison E V, Duff S M, Durkin M, FitzGerald C T, Fowler J W, Gard J D, Hilton G C, Irwin K D, Joe Y I, Morgan K M, O'Neil G C, Pappas C G, Reintsema C D, Rudman D A, Smith S J, Stevens R W, Swetz D S, Szypryt P, Ullom J N, Vale L R, Weber J C and Young B A 2019 *IEEE Trans. Appl. Supercond.* **29** 2500305

[59] Yu C, Ames A, Chaudhuri S, Dawson C, Irwin K D, Kuenstner S E, Li D and Titus C J 2020 *Eng. Res. Express* **2** 015011

[60] Yoon J, Clarke J, Gildemeister J M, Lee A T, Myers M J, Richards P L and Skidmore J T 2001 *Appl. Phys. Lett.* **78** 371

[61] Lanting T M, Cho H M, Clarke J, Dobbs M, Lee A T, Richards P L, Smith A D and Spieler H G 2003 *IEEE Trans. Appl. Supercond.* **13** 626

[62] Lanting T M, Cho H M, Clarke J, Holzapfel W L, Lee A T, Lueker M, Richards P L, Dobbs M A, Spieler H and Smith A 2005 *Appl. Phys. Lett.* **86** 112511

[63] Sakai K, Takei Y, Yamamoto R, Yamasaki N Y, Mitsuda K, Hidaka M, Nagasawa S, Kohjiro S and Miyazaki T 2014 *J. Low Temp. Phys.* **176** 400

[64] Dobbs M, Aubin F, Hann T D, Hanany S, Harrington N, Holzapfel W, Hubmayr J, Lee A, Lueker M, Macdermid K and Smecher G 2012 *J. Low Temp. Phys.* **167** 568

[65] Hattori K, Akiba Y, Arnold K, Barron D, Bender A N, Cukierman A, de Haan T, Dobbs M, Elleflot T, Hasegawa M, Hazumi M, Holzapfel W, Hori Y, Keating B, Kusaka A, Lee A, Montgomery J, Rotermund K, Shirley I, Suzuki A and Whitehorn N 2016 *J. Low Temp. Phys.* **184** 512

[66] Akamatsu H, Gottardi L, Adams J, Bailey C, Bandler S, Bruijn M, Chervenak J, Eckart M, Finkbeiner F, Hartog R, Hoevers H, Kelley R, Kuur J, Linden T, Lindeman M, Porter F, Sadleir J, Smith S, Beyer J and Kiviranta M 2013 *IEEE Trans. Appl. Supercond.* **23** 2100503

[67] Akamatsu H, Gottardi L, Adams J, Bandler S, Bruijn M, Chervenak J, Eckart M, Finkbeiner F, Hartog R, Hoevers H, Kelley R, Kilbourne C, Kurr J, Linden A J, Porter F, Sadleir J, Smith S and Kiviranta M 2014 *J. Low Temp. Phys.* **176** 591

[68] Bruijn M P, Gottardi L, den Hartog R H, Hoevers H F C, de Korte P A J and van der Kuur J 2011 *IEEE Trans. Appl. Supercond.* **21** 294

[69] Bruijn M P, Gottardi L, den Hartog R H, Hoevers H F C, Kiviranta M, de Korte P A J and van der Kuur J 2012 *J. Low Temp. Phys.* **167** 695

[70] Yamamoto R, Sakai K, Takei Y, Yamasaki N Y and Mitsuda K 2014 *J. Low Temp. Phys.* **176** 453

[71] Dobbs M A, Lueker M, Aird K A, Bender A N, Benson B A, Bleem L E, Carlstrom J E, Chang C L, Cho H-M, Clarke J, Crawford T M, Crites A T, Flanigan D I, de Haan T, George E M, Halverson N W, Holzapfel W L, Hrubes J D, Johnson B R, Joseph J, Keisler R, Kennedy J, Kermish Z, Lanting T M, Lee A T, Leitch E M, Luong-Van D, McMahon J J, Mehl J, Meyer S S, Montroy T E, Padin S, Plagge T, Pryke C, Richards P L, Ruhl J E, Schaffer K K, Schwan D, Shirokoff E, Spieler H G, Staniszewski Z, Stark A A, Vanderlinde K, Vieira J D, Vu C, Westbrook B and Williamson R 2012 *Rev. Sci. Instrum.* **83** 073113

[72] Sakai K, Yamamoto R, Takei Y, Yamasaki N Y, Mitsuda K, Miyazaki T, Hidaka M, Nagasawa S and Kohjiro S 2015 *15th International Superconductive Electronics Conference (ISEC)*, July 6–9, 2015, Nagoya, Japan, pp. 1–4

[73] Wang Q, Khosropanah P, Kuur J, Lange G D, Audley M D, Aminaei A, Hijmering R, Ridder M L, llyas S, Linden A J, Bruijn M P, Tak F and Gao J R 2021 *Rev. Sci. Instrum.* **92** 014710

[74] Hartog R, Barret D, Gottardi L, Herder J, Jackson B, Korte P, Kuur J, Leeuwen B, Loon D Nieuwenhuizen A and Ravera L 2014 *Proc. SPIE* **9144** 91445Q

[75] Hartog R D, Audley M D, Beyer J, Boersma D, Bruijn M, Gottardi L, Hoevers H, Hou R, Keizer G, Khosropanah P, Kiviranta M, Korte P, Kurr J, Leeuwen B J, Nieuwenhuizen A C T and Winden P 2012 *J. Low Temp. Phys.* **167** 652

[76] Audley M D, Wang Q, Hijmering R A, Khosropanah P, de Lange G, van der Linden A J, Ridder M L and Taralli E 2020 *J. Low Temp. Phys.* **199** 723

[77] Hahn I, Day P, Bumble B and Leduc H G 2008 *J. Low Temp. Phys.* **151** 934

[78] Mates J A B, Hilton G C, Lrwin K D, Vale L R and Lehnert K W 2008 *Appl. Phys. Lett.* **92** 023514

[79] Hirayama F, Kohjiro S, Fukuda D, Yamamori H, Nagasawa S and Hidaka M 2013 *IEEE Trans. Appl. Supercond.* **23** 2500405

[80] Kohjiro S, Hirayama F, Yamamori H, Nagasawa S, Fukuda D and Hidaka M 2014 *J. Appl. Phys.* **115** 223902

[81] Dober B, Becker D T, Bennett D A, Bryan S A, Duff S M, Gard J D, Hays-Wehle J P, Hilton G C, Hubmayr J, Mates J A B, Reintsema C D, Vale L R and Ullom J N 2017 *Appl. Phys. Lett.* **111** 243510

[82] Mates J A B, Irwin K D, Vale L R, Hilton G C, Gao J and Lehnert K W 2012 *J. Low Temp. Phys.* **167** 707

[83] Karcher N, Richter D, Ahrens F, Gartmann R, Wegner M, Krömer O, Kempf S, Enss C, Weber M and Sander O 2020 *J. Low Temp. Phys.* **200** 261

[84] Mates J A B, Becker D T, Bennett D A, Dober B J, Gard J D, Hilton G C, Swetz D S, Vale L R and Ullom J N 2019 *Appl. Phys. Lett.* **115** 202601

[85] Hirayama F, Irimatsugawa T, Yamamori H, Kohjiro S, Sato A, Nagasawa S, Fukuda D, Sasaki H, Hidaka M, Sato Y, Ohno M and Takahashi H 2017 *IEEE Trans. Appl. Supercond.* **27** 2500205

[86] Gard J D, Becker D T, Bennett D A, Fowler J W, Hilton G C, Mates J A B, Reintsema C D, Schmidt D R, Swetz D S and Ullom J N 2018 *J. Low Temp. Phys.* **193** 485

[87] Irwin K D and Lehnert K W 2004 *Appl. Phys. Lett.* **85** 2107

[88] Mates J A B, Becker D T, Bennett D A, Dober B J, Gard J D, Hays-Wehle J P, Fowler J W, Hilton G C, Reintsema C D, Schmidt D R, Swetz D S, Vale L R and Ullom J N 2017 *Appl. Phys. Lett.* **111** 062601

[89] Nakashima Y, Hirayama F, Kohjiro S, Yamamori H, Nagasawa S, Sato A, Yamada S, Hayakawa R, Yamasaki N Y, Mitsuda K, Nagayoshi K, Akamatsu H, Gottardi L, Taralli E, Bruijn M P, Ridder M L, Gao J R and den Herder J W A 2020 *Appl. Phys. Lett.* **117** 122601

[90] Nakada N, Hattori K, Nakashima Y, Hirayama F, Yamamoto R, Yamamori H, Kohjiro S, Sato A, Takahashi H and Fukuda D 2020 *J. Low Temp. Phys.* **199** 206

[91] Dober B, Ahmed Z, Arnold K, Becker D T, Bennett D A, Connors J A, Cukierman A, D'Ewart J M, Duff S M, Dusatko J E, Frisch J C, Gard J D, Henderson S W, Herbst R, Hilton G C, Hubmayr J, Li Y, Mates J A B, McCarrick H, Reintsema C D, Silva-Feaver M, Ruckman L, Ullom J N, Vale L R, Van Winkle D D, Vasquez J, Wang Y, Young E, Yu C and Zheng K 2021 *Appl. Phys. Lett.* **118** 062601